

Ov3R: Open-Vocabulary Semantic 3D Reconstruction from RGB Videos

Ziren Gong¹, Xiaohan Li², Fabio Tosi¹, Jiawei Han³, Stefano Mattoccia¹, Jianfei Cai⁴, Matteo Poggi¹

University of Bologna¹, USTC², BIT³, Monash University⁴

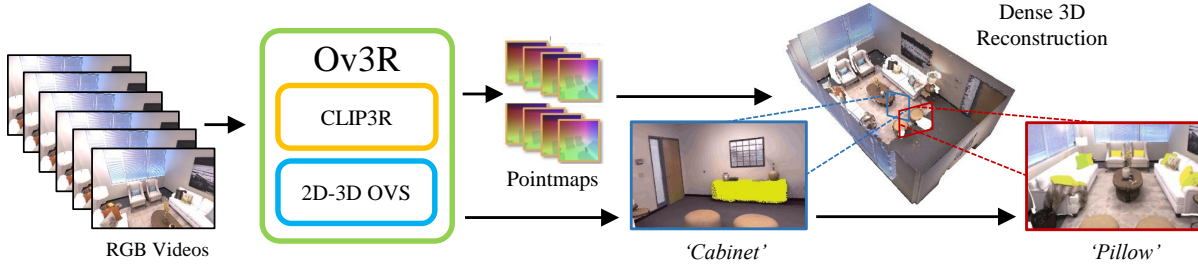


Figure 1: **Ov3R is an Open-Vocabulary Semantic 3D Reconstruction Framework.** It consists of two novel feed-forward modules, *CLIP3R* and *2D-3D OVS*, and excels in both 3D reconstruction and open-vocabulary 3D semantic segmentation.

Abstract

We present Ov3R, a novel framework for open-vocabulary semantic 3D reconstruction from RGB video streams, designed to advance Spatial AI. The system features two key components: *CLIP3R*, a CLIP-informed 3D reconstruction module that predicts dense point maps from overlapping clips while embedding object-level semantics; and *2D-3D OVS*, a 2D-3D open-vocabulary semantic module that lifts 2D features into 3D by learning fused descriptors integrating spatial, geometric, and semantic cues. Unlike prior methods, Ov3R incorporates CLIP semantics directly into the reconstruction process, enabling globally consistent geometry and fine-grained semantic alignment. Our framework achieves state-of-the-art performance in both dense 3D reconstruction and open-vocabulary 3D segmentation — marking a step forward toward real-time, semantics-aware Spatial AI.

1 Introduction

Spatial AI systems (Davison 2018) aim to understand both the geometry and semantics of the surrounding environment from images in real-time, enabling an embedded AI agent to navigate and interact with it effectively.

Dense 3D reconstruction lies at the core of these systems. Over the decades, this task has taken various forms — from Structure-from-Motion (SfM) (Lindenberger et al. 2021; Liu et al. 2023; Schonberger and Frahm 2016; Snavely, Seitz, and Szeliski 2006) and Multi-View Stereo (MVS), typically performed offline, to Simultaneous Localization and Mapping (SLAM) (Campos et al. 2021; Engel, Schöps, and Cremers 2014; Gong et al. 2025; Teed and Deng 2021), which is executed online by autonomous agents and thus requires real-time processing. The latter flavor is the most suitable approach for developing Spatial AI systems, although

it poses greater challenges compared to offline methods, as input images are collected incrementally rather than being available in advance — making the system more susceptible to noise, motion blur, and cumulative drift over time.

In the last few years, SLAM has undergone a resurgence, fueled by advancements in related fields such as novel view synthesis (Mildenhall et al. 2021; Kerbl et al. 2023) and, more recently, the emergence of 3D reconstruction models (Wang et al. 2024b) (3R), which have redefined the classical reconstruction paradigm by bypassing explicit camera pose estimation. The former has led to a family of SLAM methods, based on NeRF or 3DGS, yielding dense 3D reconstructions and accurate camera tracking, albeit with high computational cost due to the need for scene-specific training. The latter, in contrast, has resulted in the first 3R-based systems capable of real-time performance, though often at the expense of tracking accuracy, due to the absence of explicit pose estimation. In both directions, however, the semantic understanding of the surrounding environment has remained largely unexplored — and where considered, it has been limited to simplified scenarios with a predefined set of classes (Zhu et al. 2024c,b). As a result, a significant gap between existing SLAM methods and envisioned Spatial AI systems still persists.

In parallel, with the emergence of CLIP (Radford et al. 2021), research on open-vocabulary 3D semantic understanding has surged. However, existing approaches largely rely on offline reconstruction pipelines (Kerr et al. 2023; Nguyen et al. 2024; Peng et al. 2023; Qin et al. 2024; Takmaz et al. 2023; Tie et al. 2024) or RGBD SLAM methods that require depth sensors (Martins, Oswald, and Civera 2024), and therefore do not address the aforementioned gap.

In this paper, we introduce Ov3R, an open-vocabulary se-

mantic 3D reconstruction framework that processes RGB-only video streams. Ov3R comprises two key components to achieve both accurate 3D reconstruction and semantic scene understanding: (i) CLIP3R, a CLIP-informed 3R model enriched with object-level CLIP features that encode the semantics of individual objects in the scene; and (ii) 2D-3D OVS, a module that integrates rich semantic information from various foundation models — CLIP, DINO and a distilled 3D-DINO encoder — to effectively segment the dense 3D reconstruction produced by CLIP3R. These two components are loosely coupled through the CLIP features, making Ov3R a modular framework capable of performing the two tasks independently — e.g., running only 3D reconstruction when semantic understanding is not required.

Through extensive experiments on 3D reconstruction and open-vocabulary 3D segmentation, we demonstrate that Ov3R delivers high-quality dense scene reconstructions along with accurate open-vocabulary 3D semantic segmentation. Our main contributions are as follows:

- We present Ov3R, a novel framework that unifies cutting-edge 3R models and open-vocabulary 3D semantic segmentation - a bold step toward Spatial AI.
- We design CLIP3R, a CLIP-informed 3D reconstruction model that enforces semantic consistency across multi-view images and learns stronger semantic–geometric alignment.
- We propose 2D–3D OVS, a module that effectively lifts 2D CLIP descriptors into fused 2D–3D representations, enabling both spatial and geometric awareness to anchor language semantics and scene geometry.
- Ov3R achieves state-of-the-art performance in both 3D reconstruction and open-vocabulary 3D segmentation tasks.

2 Related Work

We identify two broad research areas relevant to our work.

1 3D Reconstruction

Existing approaches for this task can be divided into offline, dense SLAM, and the recent 3R-based methods.

Offline Pipelines. This category includes strategies that assume the availability of a complete set of images beforehand (Lindenberger et al. 2021; Liu et al. 2023; Schonberger and Frahm 2016; Snavely, Seitz, and Szeliski 2006), from which to process either camera parameters and 3D points via Structure from Motion (SfM) (Arrigoni 2025), or 3D points only through Multi-View Stereo (MVS) (Wang et al. 2024a). With the advent of NeRF (Mildenhall et al. 2021) and 3DGS (Kerbl et al. 2023) for novel view synthesis, several derived frameworks (Li et al. 2023b; Chen et al. 2024b,c; Guédon and Lepetit 2024; Chen et al. 2024a) have been developed to achieve high-fidelity 3D reconstructions. However, offline processing does not fulfill the requirements of a Spatial AI system.

SLAM Systems. These approaches estimate the camera pose and the 3D structure of the environment during navigation – i.e., while images are being collected in real-time. Early hand-crafted works (Campos et al. 2021; Teed and Deng 2021; Bailey and Durrant-Whyte 2006; Durrant-Whyte and Bailey 2006; Engel, Schöps, and Cremers 2014) focused mostly on camera tracking, while yielding sparse 3D reconstructions. More recently, the integration of novel views synthesis techniques (NeRF and 3DGS) into SLAM (Tosi et al. 2024) has enabled both accurate and dense reconstructions, either assuming the availability of depth sensors (Zhang et al. 2023; Li, Liu, and Wu 2024; Li et al. 2021) or not (Zhang et al. 2023; Zhu et al. 2024d; Li et al. 2023a; Zhu et al. 2024a; Li et al. 2023a). Although some of these frameworks have been enhanced with semantics understanding (Zhu et al. 2024c,b), their scope is often limited to a fixed set of classes and lacks real-time capabilities.

3R-driven Models. DUS3R (Wang et al. 2024b) pioneered the first end-to-end model for 3D reconstruction from two uncalibrated RGB images, predicting two pointmaps aligned to the same reference system, from which intrinsic and extrinsic camera parameters can also be derived. Several extensions of DUS3R target explicit features matching (Leroy, Cabon, and Revaud 2024), novel view synthesis (Wang et al. 2025), dynamic scene reconstructions (Zhang et al. 2024), although not achieving real-time performance. To address these limitations, Spann3R (Wang and Agapito 2024) introduces an incremental reconstruction approach without global alignment, enabling fast real-time operation. However, it rapidly accumulates drift errors and produces poor reconstruction accuracy. On the same track, SLAM3R (Liu et al. 2025) revisits SLAM by proposing a real-time 3D reconstruction method that does not require explicit pose estimation. Nonetheless, current 3R-based frameworks remain focused on detailed geometry reconstruction, disregarding higher-level scene understanding.

2 3D Open Vocabulary Semantics

Closed-vocabulary Online Semantics. These methods predict per-pixel segmentation using pre-defined classes. SemanticFusion pioneered per-pixel 3D semantic prediction from multi-view images. Recently, several semantic SLAM methods have been introduced to simultaneously reconstruct dense maps and semantics. NIS-SLAM (Zhai et al. 2024) integrates semantics into tri-plane features to optimize both scene representation and semantic predictions. SGS-SLAM (Li et al. 2024) and NEDS-SLAM (Ji et al. 2024) encode semantics into Gaussians and incrementally reconstruct scenes with a closed-set segmentation. These methods achieve scene understanding by assuming a known set of 2D semantic annotations. However, relying on pre-defined semantic classes limits their applicability in real-world scenarios where novel object categories may appear.

3D Open-Vocabulary Offline Semantics. Most open-vocabulary semantic methods rely heavily on pre-processed 3D scene points as input. OpenScene (Peng et al. 2023) encodes per-pixel dense features in CLIP feature space and associates 2D dense features with known 3D scene points. Open3DIS (Nguyen et al. 2024) relies significantly on pre-

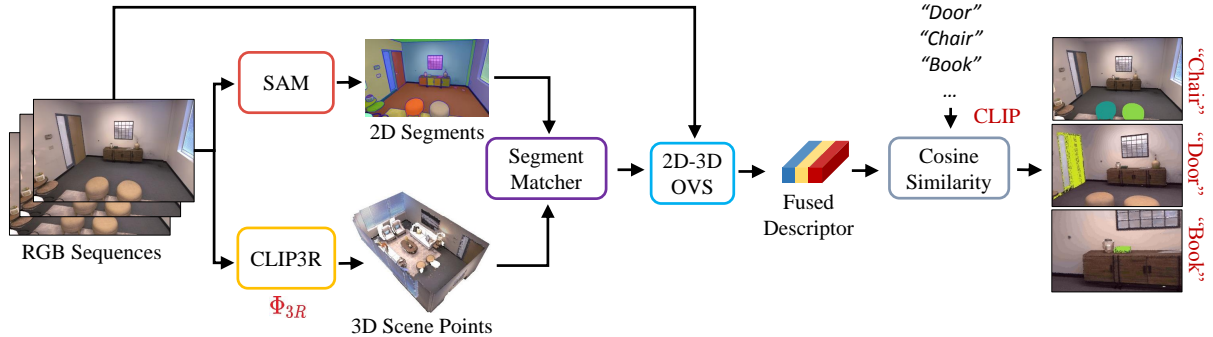


Figure 2: **Overview of Ov3R.** Given RGB-only videos, we first apply CLIP3R to produce scene points while SAM predicts 2D segments. Each 2D segment is matched to its corresponding 3D points to obtain 3D semantics. Next, the 2D-3D OVS extracts the fused 2D-3D descriptor to compute the cosine similarity with the text embeddings corresponding to a set of semantic classes.

processed 2D and 3D semantic instances to extract point-wise features. Unlike these approaches that require known 3D points, OpenNeRF (Engelmann et al. 2024) directly uses RGB images as input for NeRF and OpenSeg (Ghiasi et al. 2022). Similarly, HOV-SG (Werby et al. 2024) extracts 3D semantics and scene graph hierarchy from RGB-D sequences, relying heavily on feature pre-processing. Unlike the above offline methods, OVO (Martins, Oswald, and Civera 2024) proposes the first online 3D open-vocabulary semantic mapping compatible with SLAM systems. It can extract and track 3D segments from RGB-D videos while encoding CLIP descriptors through a proposed CLIP merging strategy. However, it still requires depth information and explicit pose estimation from SLAM systems. Besides, OVO computes CLIP descriptors solely from 2D images, overlooking the potential of 3D geometric information. In contrast, our Ov3R can extract 3D segments without depth sensors or explicit camera tracking. Additionally, we introduce a 2D-3D OVS module integrating DINO features and 3D information into CLIP descriptors.

3 Method

We now introduce Ov3R, whose overall architecture is depicted in Figure 2. It consists of two main components, highlighted in red in the figure: (i) a CLIP-informed 3R-based model (CLIP3R) and (ii) a 2D-3D OVS module. CLIP3R produces dense scene points with semantic alignment in real-time, while 2D-3D OVS serves as a downstream task – open-vocabulary semantic segmentation. It enables Ov3R to reconstruct 3D semantic scenes while retaining the possibility to perform two tasks independently.

1 CLIP3R

We introduce CLIP3R, a CLIP-informed 3D reconstruction model that integrates the rich semantic understanding embedded in CLIP features and enables open-vocabulary semantic segmentation as a downstream task thanks to the image-text alignment. It can be formalized as a model Φ_{3R} that processes multi-view RGB sequences $I_i^{(H \times W \times 3)}$ to pre-

dict dense point maps $P_i^{(H \times W \times 3)}$:

$$\Phi_{3R} \left(I_i^{(H \times W \times 3)} \right) \rightarrow P_i^{(H \times W \times 3)}, i = 1, \dots, L \quad (1)$$

As shown in Figure 3, inspired by (Liu et al. 2025), CLIP3R deploys two main branches: an Image-to-Points (I2P, in yellow) model and a Local-to-World (L2W, in blue) model.

1) The former is a ViT, inspired by DUS3R that runs over a local window of images to predict a pointmap aligned to the reference system of the central frame (i.e., the keyframe). This is achieved by processing images with a shared encoder E_{img} and two decoders D_{key} and D_{sup} for the keyframe and remaining images, respectively. Notably, no explicit camera pose estimation is performed, which in turn can be derived from the pointmap as a byproduct.

2) The latter, instead, processes the local pointmaps and aligns them to the scene-level reconstruction. It employs a pointmap encoder E_{pts} , a registration decoder D_{reg} , and a scene decoder D_{sce} , sharing the same structure as the encoder and decoder used by I2P. It identifies correlated keyframes using a reservoir and retrieval strategy (Liu et al. 2025) and processes them to predict global scene points \hat{P}_i .

Both branches, however, lack high-level reasoning about scene semantics, which we address through integration of CLIP features and CLIP-semantic supervision, to learn a stronger semantic-geometric relationship and semantic consistency.

Object-level CLIP features. Although rich in semantics, CLIP embeddings are image-level features and therefore fail at modeling the fine-grained semantics of individual objects in the scene (Zuo et al. 2025). To overcome this limitation, we extract object-level CLIP features $f_{oCLIP}^{(H \times W \times D)}$ in place of vanilla CLIP features. This is achieved by first obtaining M object masks $m^{(H \times W \times 1)}$ using the Segment Anything Model (SAM) (Kirillov et al. 2023). We then create M masked images and process them to extract CLIP patch embeddings, which are averaged and upsampled to $f_{CLIP}^{(H \times W \times D)}$ to match the image resolution. Finally, the object-level features $f_{oCLIP}^{(H \times W \times D)}$ are obtained by combining the individual CLIP features obtained from the M masked images within a single features map as:

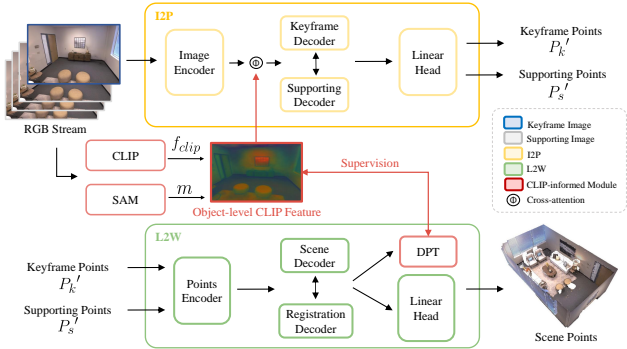


Figure 3: **CLIP3R Overview.** I2P integrates object-level CLIP features with visual embeddings to predict local pointmaps. L2W then aligns these local pointmaps to global scene coordinates while predicting object-level CLIP features in scene space.

$$f_{oCLIP}^{(H \times W \times D)} = \sum_{i=0}^M m_i^{(H \times W \times 1)} \cdot f_{CLIP_i}^{(H \times W \times D)} \quad (2)$$

These finer-level features are then integrated into CLIP3R.

CLIP-informed I2P. To predict local pointmaps, the I2P branch extracts visual tokens $F_{vit}^{(T \times d)}$ from each frame in the processed window through ViT blocks (Dosovitskiy et al. 2020). To enrich I2P with knowledge from CLIP, we concurrently extract object-level CLIP features and tokenize them into $F_{oCLIP}^{(T \times d)}$. Then, F_{oCLIP} and F_{vit} are processed through cross-attention to obtain the fused features F_{fuse} , which are added to F_{vit} . The encoding process is denoted as:

$$F_{fuse} = F_{vit} + \text{softmax}\left(\frac{F_{vit} F_{oCLIP}}{\sqrt{F_{oCLIP}}}\right) F_{oCLIP} \quad (3)$$

These features are then processed by the keyframe decoder D_{key} and the supporting decoder D_{sup} from the original I2P. A linear head is applied to predict both scene points P'_i ($P'_k, P'_s \in P'_i$) and confidence map C . The revised I2P network is trained end-to-end through a confidence-aware loss over ground truth scene points:

$$L_{I2P} = \sum_{i=1}^L M_i \cdot (C \cdot L1\left(\frac{1}{z'} P'_i, \frac{1}{z} P_i\right) - \alpha \log C) \quad (4)$$

where L is the number of supporting frames, M_i are the masked points with ground truth values in P_i , $L1$ is the point-wise Euclidean distance, z and z' are scale factors, and α is a hyperparameter controlling the regularization term.

CLIP-informed L2W. The L2W branch maintains its original structure but incorporates an additional prediction head for object-level CLIP features f'_{oCLIP} . This head embeds fine-grained semantic knowledge directly into the final 3D reconstruction while enforcing semantic consistency across the scene. This head is implemented as a DPT (Ranftl, Bochkovskiy, and Koltun 2021), and the entire L2W branch is trained using two losses: L_{L2W} and L_{oCLIP} . The former is similar to the loss used to supervise I2P:

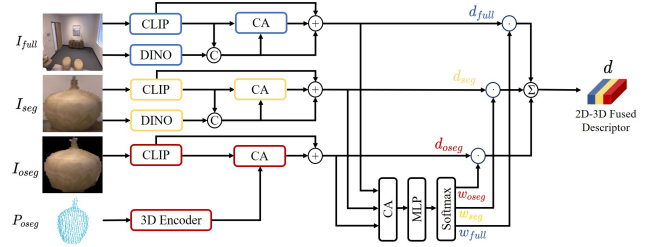


Figure 4: **2D-3D OVS Overview.** After matching 2D and 3D segments across images and pointmaps, CLIP, DINO, and 3D features are combined into a 2D-3D fused descriptor.

$$L_{L2W} = \sum_{i=1}^L M_i \cdot (\hat{C} \cdot L1(\hat{P}'_i, P_i) - \alpha \log \hat{C}) \quad (5)$$

while the latter minimizes the feature distance between extracted f_{oCLIP} and predicted f'_{oCLIP} features:

$$L_{oCLIP} = \left\| f'_{oCLIP} - f_{oCLIP} \right\|_1 \quad (6)$$

2 2D-3D OVS

We now introduce the second core component of Ov3R, responsible for performing open-vocabulary 3D semantic segmentation over the 3D reconstruction produced by CLIP3R.

3D Segments Matching. We adopt the strategy from (Martins, Oswald, and Civera 2024): after predicting dense point maps for each frame, we generate 2D object masks from images using SAM (Kirillov et al. 2023). We then project the 3D point map onto each keyframe and assign a 2D segment labels, corresponding to the SAM-predicted masks, to the matched 3D points. After processing all 2D segments, 3D points sharing the same label are merged into coherent 3D segments. However, this strategy relies solely on 2D information and lacks explicit semantic knowledge from the 3D geometry itself. To address this limitation, we introduce 2D-3D fused descriptors, obtained as follows.

2D-3D Fused Descriptors. CLIP features alone are insufficient to model semantics in 3D space, as they lack fine-grained details and clear object boundaries. While DINO (Caron et al. 2021) features extract clear boundaries between inter-components, they lack knowledge about 3D geometry – which is, on the contrary, available from point features (Hegde, Valanarasu, and Patel 2023) extracted from 3D pointclouds. Therefore, we introduce a 2D-3D fused descriptor that combines these three complementary features types extracted from CLIP, DINO, and a 3D-CLIP encoder (Hegde, Valanarasu, and Patel 2023).

To capture contextual information, we adopt the multi-level architecture by (Werby et al. 2024) and (Martins, Oswald, and Civera 2024), as shown in Figure 4. From each keyframe, we extract CLIP and DINO features at three levels: from the full frame I_{full} and from a crop containing the 2D segment (w/ background) I_{seg} , while encoding CLIP and 3D points features after masking the crop to remove background I_{oseg} (w/o background), and its corresponding

Method	Room0 Acc. / Comp.	Room1 Acc. / Comp.	Room2 Acc. / Comp.	Office0 Acc. / Comp.	Office1 Acc. / Comp.	Office2 Acc. / Comp.	Office3 Acc. / Comp.	Office4 Acc. / Comp.	Average Acc. / Comp.	ATE RMSE	FPS
DUS3R	3.47 / 2.50	2.53 / 1.86	2.95 / 1.76	4.92 / 3.51	3.09 / 2.21	4.01 / 3.10	3.27 / 2.25	3.66 / 2.61	3.49 / 2.48	4.76	<1
MAS3R	4.01 / 4.10	3.61 / 3.25	3.13 / 2.15	2.57 / 1.63	12.85 / 8.13	3.13 / 1.99	4.67 / 3.15	3.69 / 2.47	4.71 / 3.36	1.67	<<1
NICER-SLAM	2.53 / 3.04	3.93 / 4.10	3.40 / 3.42	5.49 / 6.09	3.45 / 4.42	4.02 / 4.29	3.34 / 4.03	3.03 / 3.87	3.65 / 4.16	1.88	<<1
DROID-SLAM	12.18 / 8.96	8.35 / 6.07	3.26 / 16.01	3.01 / 16.19	2.39 / 16.20	5.66 / 15.56	4.49 / 9.73	4.65 / 9.63	5.50 / 12.29	0.33	20
DIM-SLAM	14.19 / 6.24	9.56 / 6.45	8.41 / 12.17	10.16 / 5.95	7.86 / 8.33	16.50 / 8.28	13.01 / 6.77	13.08 / 8.62	11.60 / 7.85	0.46	3
MGS-SLAM	-	-	-	-	-	-	-	-	7.51 / 3.64	0.32	0.6
GO-SLAM	-	-	-	-	-	-	-	-	3.81 / 4.79	0.39	8
Spann3R	9.75 / 12.94	15.51 / 12.94	7.28 / 8.50	5.46 / 18.75	5.24 / 16.64	9.33 / 11.80	16.00 / 9.03	13.97 / 16.02	10.32 / 13.33	32.79	>50
SLAM3R	3.19 / 2.40	3.12 / 2.34	2.72 / 2.00	4.28 / 2.60	3.17 / 2.34	3.84 / 2.78	3.90 / 3.16	4.32 / 3.36	3.57 / 2.62	6.61	24
Ov3R(Ours)	2.67 / 1.98	2.96 / 1.83	2.67 / 1.91	3.41 / 2.24	3.24 / 2.23	3.24 / 2.16	3.21 / 2.36	2.99 / 2.25	3.05 / 2.12	6.00	15

Table 1: **3D reconstruction and tracking results on Replica**. Methods are grouped into: 3R-driven methods with low FPS, SLAM-based approaches, and real-time 3R-driven frameworks. We highlight the **first**, **second**, and **third** best results.



Figure 5: **Qualitative results – Dense Pointmaps on Replica**. Compared to competing methods, Ov3R demonstrates superior completeness and geometric alignment, particularly visible in the reconstruction of **chairs (blue)** and **desks (yellow)**.

portion of the pointmap P_{oseg} . In the first two branches, the DINO features F_{dino} ($F_{dino}^f, F_{dino}^s \in F_{dino}$) extracted through ViT-small architecture (Caron et al. 2021) are first projected to the same feature dimension as CLIP features by a linear layer. The DINO features are then concatenated with CLIP features F_{clip} ($F_{clip}^f, F_{clip}^s \in F_{clip}$), followed by a linear layer to transform the dimensions:

$$F_{cat} = \text{Linear}([F_{dino}, F_{clip}]) \quad (7)$$

Subsequently, the concatenated features F_{cat} ($F_{cat}^f, F_{cat}^s \in F_{cat}$) and CLIP features are processed through cross-attention (CA) to obtain the features $F_{atten-cd}$, guided by the spatial structure in DINO features. We sum up CLIP features, DINO features, and the refined CLIP features to represent the descriptors of I_{full} and I_{seg} as:

$$d_{full} = F_{clip}^f + F_{cat}^f + \text{softmax}\left(\frac{F_{cat}^f F_{clip}^f}{F_{clip}^f}\right) F_{clip}^f \quad (8)$$

$$d_{seg} = F_{clip}^s + F_{cat}^s + \text{softmax}\left(\frac{F_{cat}^s F_{clip}^s}{F_{clip}^s}\right) F_{clip}^s \quad (9)$$

where d_{full} and d_{seg} denote the descriptors of the full frame I_{full} and the image crop containing the 2D segment (w/ background) I_{seg} , respectively. In the third branch, we introduce a CLIP-like distilled 3D point encoder (Hegde, Valanarasu, and Patel 2023) to extract geometric features. This 3D encoder is pre-trained on triplets of pointclouds, corresponding images, and text using natural language supervision. The 3D features obtained by this distilled encoder naturally align with the CLIP latent space. Accordingly, we first obtain the 3D segment P_{oseg} corresponding to the 2D segment (w/o background) I_{oseg} . Then, the 3D features F_{point}^{os} ,

processed by a linear layer, are fed into cross-attention with CLIP features F_{clip}^{os} to learn semantic-geometric relationships. We add the geometry-informed features to the CLIP features to represent the descriptor of I_{oseg} :

$$d_{oseg} = F_{clip}^{os} + \text{softmax}\left(\frac{F_{point}^{os} F_{clip}^{os}}{F_{clip}^{os}}\right) F_{clip}^{os} \quad (10)$$

where d_{oseg} denotes the descriptor of the image crop only with the 2D segment I_{oseg} . We employ the same weighted merging strategy from (Martins, Oswald, and Civera 2024) to combine these three features from different levels:

$$d = \sum^i w_i \odot d_i, i = \text{full, seg, oseg} \quad (11)$$

where d is our 2D-3D fused descriptor. \odot denotes the Hadamard product. The weights w_i are obtained by a shallow model comprising a cross-attention layer, an MLP, and a softmax layer. We pre-trained our 2D-3D fusion model by minimizing the sigmoid cosine similarity loss:

$$L_{sim} = -\frac{1}{|B|} \sum_i^{|B|} \sum_j^{|B|} \log \left(\frac{1}{1 + \exp(z_{ij}(-kd_i \cdot t_j + b))} \right) \quad (12)$$

where B is a mini-batch containing pairs of 2D segments and semantic labels. z_{ij} is a binary label (1 or -1) indicating whether the segment and semantic label are paired. t_j is the text embedding encoded by CLIP. k and b are learnable bias and temperature parameters, respectively. At inference time, the similarity between fused descriptors and a set of text embeddings corresponding to semantic classes is computed: the class with the highest similarity is finally selected.

Method	Chess Acc. / Comp.	Fire Acc. / Comp.	Heads Acc. / Comp.	Office Acc. / Comp.	Pumpkin Acc. / Comp.	RedKitchen Acc. / Comp.	Stairs Acc. / Comp.	Average Acc. / Comp.	ATE RMSE	FPS
DUS3R	2.26 / 2.13	1.04 / 1.50	1.66 / 0.98	4.62 / 4.74	1.73 / 2.43	1.95 / 2.36	3.37 / 10.75	2.19 / 3.24	8.02	<1
MAS3R	2.08 / 2.12	1.54 / 1.43	1.06 / 1.04	3.23 / 3.19	5.68 / 3.07	3.50 / 3.37	2.36 / 13.16	3.04 / 3.90	6.28	<<1
Spann3R	2.23 / 1.68	0.88 / 0.92	2.67 / 0.98	5.86 / 3.54	2.55 / 1.85	2.68 / 1.80	5.65 / 5.15	3.42 / 2.41	11.7	>50
SLAM3R	1.63 / 1.31	0.84 / 0.83	2.95 / 1.22	2.32 / 2.26	1.81 / 2.05	1.84 / 1.94	4.19 / 6.91	2.13 / 2.34	8.41	25
Ov3R(Ours)	1.53 / 1.26	0.79 / 0.76	2.41 / 0.99	1.95 / 1.93	1.66 / 1.89	1.63 / 1.82	3.88 / 5.95	1.98 / 2.08	7.71	17

Table 2: **3D reconstruction and tracking results on 7Scenes dataset.** The results are divided into two groups: 3R-driven methods with low FPS, and real-time 3R-driven frameworks.

Method	All mIoU / mAcc	Head mIoU / mAcc	Common mIoU / mAcc	Tail mIoU / mAcc
Geometry: GT				
OpenScene	15.9 / 24.6	31.7 / 44.8	14.5 / 22.6	1.5 / 6.3
OpenNeRF	20.4 / 31.7	35.4 / 46.2	20.1 / 31.3	5.8 / 17.6
HOV-SG	22.5 / 34.2	35.9 / 44.2	23.6 / 42.3	8.0 / 16.1
Open3DIS	25.6 / 38.7	49.7 / 64.4	22.1 / 42.4	4.9 / 9.4
O ₂ V-mapping	7.8 / 13.9	19.3 / 27.5	4.0 / 6.7	0.1 / 7.5
OVO-mapping	26.5 / 35.8	41.0 / 52.3	21.1 / 31.8	17.6 / 23.2
Ov3R(Ours)	30.7 / 41.3	43.1 / 55.3	27.1 / 38.0	21.8 / 30.6
Geometry: CLIP3R				
OVO-CLIP3R	25.6 / 34.9	39.3 / 51.0	20.5 / 31.1	17.1 / 22.8
Ov3R(Ours)	30.0 / 40.8	42.0 / 54.3	26.5 / 37.6	21.5 / 30.6

Table 3: **Open-vocabulary 3D semantic segmentation results on Replica dataset.** On top: methods running on ground truth 3D reconstructions. At the bottom: methods running on CLIP3R reconstructions.

4 Experiments

Datasets. For the 3D reconstruction task, we train CLIP3R on ScanNet++ (Yeshwanth et al. 2023), Aria Synthetic Environments (Avetisyan et al. 2024), and CO3D-v2 (Reizenstein et al. 2021), which provide diverse scenarios and objects from both real-world and synthetic scenes. We evaluate 3D reconstruction performance on Replica (Straub et al. 2019) and 7Scenes (Shotton et al. 2013). For the open-vocabulary 3D segmentation task, we train the 2D-3D OVS module on ScanNet++ and evaluate it on Replica and ScanNetv2 (Dai et al. 2017). Additionally, we report camera tracking results from CLIP3R on both Replica and 7Scenes.

Metrics. We adopt standard metrics including *Accuracy (cm)*, *completion (cm)* for 3D reconstruction, *Absolute Trajectory Error (ATE RMSE)* for tracking accuracy, and *Frame Per Second (FPS)* to assess efficiency. For open-vocabulary 3D segmentation, we use *mean Intersection Over Union (mIoU)* and *mean Accuracy (mAcc)* between the ground truth 3D labels and the labeled vertices of 3D meshes. Additionally, we evaluate label-frequency weighted metrics (f-mIoU and f-mAcc) for ScanNetv2.

Implementation Details. Ov3R is trained on 4 NVIDIA A100 GPU, each with 64 GB of memory, while inference can be performed on a single 3090 NVIDIA GPU with 24 GB of memory. In CLIP3R, we set 24 encoder blocks and 12 decoder blocks with linear heads, setting the window length to $L = 5$ for initialization and $L = 11$ for subsequent incremental windows. The 2D-3D OVS model is trained for 15 epochs, with batch size 512. We use SAM 2.1 for 2D instance segmentation, SigLip ViT-SO400 for CLIP features,

Methods	ScanNet20				ScanNet200			
	mIoU	mAcc	f-mIoU	f-mAcc	mIoU	mAcc	f-mIoU	f-mAcc
Geometry: GT								
OpenScene	44.6	61.9	57.6	71.0	9.4	12.6	27.8	32.0
HOV-SG	34.4	51.1	47.3	61.8	11.2	18.7	27.7	37.6
Open3DIS	37.3	52.8	57.0	67.9	17.8	23.7	27.9	34.1
OVO-mapping	38.1	50.5	57.6	70.5	17.2	25.3	45.4	56.4
Ov3R(Ours)	42.3	56.2	63.8	77.4	18.6	27.6	49.5	60.8
Geometry: CLIP3R								
OVO-CLIP3R	32.6	44.2	48.9	64.8	14.1	21.5	38.0	51.2
Ov3R(Ours)	36.4	47.5	55.8	67.6	16.8	25.0	44.9	55.7

Table 4: **Open-vocabulary 3D semantic segmentation results on ScanNetv2.** On top: methods running on ground truth 3D reconstructions. At the bottom: methods running on CLIP3R reconstructions.

ViTS-16 for DINO features, and PointMLP-1024 for 3D point features.

1 3D Reconstruction

We start by assessing the quality of 3D reconstructions produced by Ov3R against state-of-the-art methods.

Replica. Table 1 compares Ov3R against the state-of-the-art reconstruction methods on 8 scenes from Replica, including both SLAM-based and 3R-based approaches. Overall, Ov3R outperforms all state-of-the-art methods while maintaining up to 15 FPS processing speed. Although Spann3R achieves up to 50 FPS, it fails to provide accurate and complete 3D reconstructions, as shown in Figure 5. In contrast, Ov3R achieves consistently superior reconstructions compared to both Spann3R and SLAM3R.

7Scenes. Table 2 reports the evaluation on the 7Scenes dataset, carried out by uniformly sampling one-twentieth of the frames from each test sequence following (Liu et al. 2025). As shown in the table, on average, Ov3R surpasses all of the baselines in both accuracy and completion, confirming the trends already highlighted on the Replica dataset.

2 Camera Tracking

Although 3R models do not explicitly estimate trajectories, camera poses can be derived from their predicted scene points. Following (Wang et al. 2024b), we extract poses by running PnP-RANSAC (Fischler and Bolles 1981) from the predicted 3D points, given the known camera intrinsics of each frame. Accordingly, we assess the tracking performance of Ov3R on the Replica and 7Scenes datasets. As shown in Table 1 and Table 2, Ov3R outperforms the other two real-time 3R-based frameworks, Spann3R and

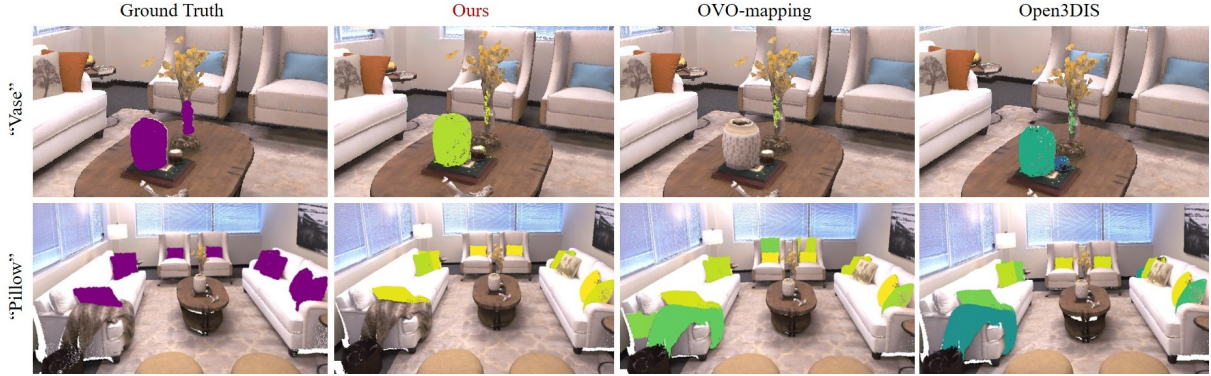


Figure 6: **Visualization of open-vocabulary 3D queries on the Replica.** We visualize two queries from “*Head*” and “*Common*” in *room0*. The similarities of queries are shown from *low* (blue) to *mid* (green), and *high* (yellow). OVO yields wrong “*Pillows*” and the missing “*Vase*”, while Open3DIS also produces wrong “*Pillows*” and low-similarity “*Vase*”.

	Acc.	Comp.	RMSE
(A) w/o CLIP-insert	3.31	2.35	6.46
(B) w/o CLIP head	3.20	2.21	6.32
Ov3R (all)	3.05	2.12	6.00

Table 5: **Ablation study of CLIP3R on Replica.** We study the impact of CLIP-insertion in I2P (CLIP-insert) and the CLIP-semantic supervision in L2W (CLIP head).

SLAM3R, narrowing the gap between this novel family of methods and the much slower dense SLAM systems.

3 Open-Vocabulary 3D Semantic Segmentation

We continue our evaluation by focusing on the open-vocabulary 3D semantic segmentation task. We conduct experiments under two different settings: segmentation performed on geometry reconstructed from (i) ground truth depth maps, simulating an offline setting, and (ii) RGB-only videos processed by CLIP3R.

Replica. We run experiments on the 8 standard scenes of Replica, annotated with 51 different semantic classes, and evaluate the results directly in 3D space rather than by projecting semantic masks onto 2D images (Kerr et al. 2023). Following (Engelmann et al. 2024), these labels are divided into three categories (“*Head*”, “*Common*”, “*Tail*”) according to their frequency in the dataset. Thanks to its modular design, we compare Ov3R with both offline approaches and the recent online method, OVO (Martins, Oswald, and Civera 2024). In Table 3, Ov3R outperforms all baselines on *mIoU* and *mAcc* across *All* labels on average, achieving the best trade-off across all categories. Although Open3DIS achieves better performance on “*Head*” labels, it fails on less frequent objects. As shown in Figure 6, Ov3R accurately identifies the queried semantic classes, whereas OVO and Open3DIS produce inaccurate segmentation or miss objects entirely.

ScanNetv2. We continue the experiments on 5 scenes from ScanNetv2, using both the original (20) and extended (200) classes. Table 4 shows that Ov3R surpasses all baselines on the ScanNet200 dataset, demonstrating its generalization capability even with diverse and previously unseen class annotations. For the ScanNet20 dataset, Ov3R outperforms other methods in terms of *f-mIoU* and *f-mAcc* over

	mIoU	mAcc	f-mIoU	f-mAcc
(C) w/o DINO	28.05	35.63	53.46	66.59
(D) w/o 3D encoder	28.46	36.20	52.81	65.38
Ov3R (all)	30.65	41.31	54.64	67.61

Table 6: **Ablation study of 2D-3D OV.** We report the advancement brought by different fusion strategies.

ground truth reconstructions, while achieving comparable results to OpenScene in *mIoU* and *mAcc*. Notably, OpenScene performance significantly deteriorates when evaluated on a much larger set of classes. Consistently, Ov3R outperforms OVO in the online setting across both datasets.

4 Ablation Study

We conclude our experiments by assessing the impact of different sub-modules on 3D reconstruction and open-vocabulary 3D semantic segmentation.

CLIP3R Component Analysis. We first assess the effects of our CLIP-informed strategy. As shown in Table 5, retaining only CLIP-semantic supervision (A) yields significant drops in both reconstruction accuracy and camera tracking, demonstrating the importance of CLIP cues in the reconstruction model. Moreover, removing the additional supervision (B) leads to consistently lower performance, confirming its key role in CLIP3R for 3D reconstruction.

2D-3D OVS Component Analysis. Table 6 shows that either CLIP descriptors fused with 3D features only (C) or those fused with DINO features only (D) lead to drops in accuracy. In contrast, our full 2D-3D OVS achieves the best performance, demonstrating that combining both 2D and 3D descriptors is crucial for accurate 3D segmentation.

5 Conclusion

We presented Ov3R, an open-vocabulary semantic 3D reconstruction framework. Compared to recent methods, Ov3R learns stronger semantic-geometric relationships and enforces semantic consistency through the proposed CLIP3R. Moreover, the introduced 2D-3D OVS enhances CLIP descriptors with spatial and geometric awareness. Our experiments demonstrate the superior accuracy and completeness of 3D reconstructions and 3D open-vocabulary semantic segmentation achieved by our approach.

Limitations and Future Work. Ov3R inherits one of the limitations of 3R models, i.e., the suboptimal accuracy of the retrieved camera poses. Future research will aim to overcome this limitation by integrating techniques from the SLAM literature, such as global bundle adjustment.

References

Arrigoni, F. 2025. A Taxonomy of Structure from Motion Methods. *arXiv preprint arXiv:2505.15814*.

Avetisyan, A.; Xie, C.; Howard-Jenkins, H.; Yang, T.-Y.; Aroudj, S.; Patra, S.; Zhang, F.; Frost, D.; Holland, L.; Orme, C.; et al. 2024. Scenescrit: Reconstructing scenes with an autoregressive structured language model. In *European Conference on Computer Vision*, 247–263. Springer.

Bailey, T.; and Durrant-Whyte, H. 2006. Simultaneous localization and mapping (SLAM): Part II. *IEEE robotics & automation magazine*, 13(3): 108–117.

Campos, C.; Elvira, R.; Rodríguez, J. J. G.; Montiel, J. M.; and Tardós, J. D. 2021. Orb-slam3: An accurate open-source library for visual, visual-inertial, and multimap slam. *IEEE transactions on robotics*, 37(6): 1874–1890.

Caron, M.; Touvron, H.; Misra, I.; Jégou, H.; Mairal, J.; Bojanowski, P.; and Joulin, A. 2021. Emerging properties in self-supervised vision transformers. In *Proceedings of the IEEE/CVF international conference on computer vision*, 9650–9660.

Chen, D.; Li, H.; Ye, W.; Wang, Y.; Xie, W.; Zhai, S.; Wang, N.; Liu, H.; Bao, H.; and Zhang, G. 2024a. PGSR: Planar-based Gaussian Splatting for Efficient and High-Fidelity Surface Reconstruction. *arXiv preprint arXiv:2406.06521*.

Chen, Y.; Xu, H.; Zheng, C.; Zhuang, B.; Pollefeys, M.; Geiger, A.; Cham, T.-J.; and Cai, J. 2024b. Mvsplat: Efficient 3d gaussian splatting from sparse multi-view images. In *European Conference on Computer Vision*, 370–386. Springer.

Chen, Y.; Zheng, C.; Xu, H.; Zhuang, B.; Vedaldi, A.; Cham, T.-J.; and Cai, J. 2024c. Mvsplat360: Feed-forward 360 scene synthesis from sparse views. *Advances in Neural Information Processing Systems*, 37: 107064–107086.

Dai, A.; Chang, A. X.; Savva, M.; Halber, M.; Funkhouser, T.; and Nießner, M. 2017. Scannet: Richly-annotated 3d reconstructions of indoor scenes. In *Proceedings of the IEEE conference on computer vision and pattern recognition*, 5828–5839.

Davison, A. J. 2018. FutureMapping: The computational structure of spatial AI systems. *arXiv preprint arXiv:1803.11288*.

Dosovitskiy, A.; Beyer, L.; Kolesnikov, A.; Weissenborn, D.; Zhai, X.; Unterthiner, T.; Dehghani, M.; Minderer, M.; Heigold, G.; Gelly, S.; et al. 2020. An image is worth 16x16 words: Transformers for image recognition at scale. *arXiv preprint arXiv:2010.11929*.

Durrant-Whyte, H.; and Bailey, T. 2006. Simultaneous localization and mapping: part I. *IEEE robotics & automation magazine*, 13(2): 99–110.

Engel, J.; Schöps, T.; and Cremers, D. 2014. LSD-SLAM: Large-scale direct monocular SLAM. In *European conference on computer vision*, 834–849. Springer.

Engelmann, F.; Manhardt, F.; Niemeyer, M.; Tateno, K.; Pollefeys, M.; and Tombari, F. 2024. OpenNeRF: open set 3D neural scene segmentation with pixel-wise features and rendered novel views. *arXiv preprint arXiv:2404.03650*.

Fischler, M. A.; and Bolles, R. C. 1981. Random Sample Consensus: A Paradigm for Model Fitting with Applications to Image Analysis and Automated Cartography. *Communications of the ACM*, 24(6): 381–395.

Ghiasi, G.; Gu, X.; Cui, Y.; and Lin, T.-Y. 2022. Scaling open-vocabulary image segmentation with image-level labels. In *European conference on computer vision*, 540–557. Springer.

Gong, Z.; Tosi, F.; Zhang, Y.; Mattoccia, S.; and Poggi, M. 2025. HS-SLAM: Hybrid Representation with Structural Supervision for Improved Dense SLAM. *arXiv preprint arXiv:2503.21778*.

Guédon, A.; and Lepetit, V. 2024. Sugar: Surface-aligned gaussian splatting for efficient 3d mesh reconstruction and high-quality mesh rendering. In *Proceedings of the IEEE/CVF Conference on Computer Vision and Pattern Recognition*, 5354–5363.

Hegde, D.; Valanarasu, J. M. J.; and Patel, V. 2023. Clip goes 3d: Leveraging prompt tuning for language grounded 3d recognition. In *Proceedings of the IEEE/CVF International Conference on Computer Vision*, 2028–2038.

Ji, Y.; Liu, Y.; Xie, G.; Ma, B.; Xie, Z.; and Liu, H. 2024. Neds-slam: A neural explicit dense semantic slam framework using 3d gaussian splatting. *IEEE Robotics and Automation Letters*.

Kerbl, B.; Kopanas, G.; Leimkühler, T.; and Drettakis, G. 2023. 3d gaussian splatting for real-time radiance field rendering. *ACM Trans. Graph.*, 42(4): 139–1.

Kerr, J.; Kim, C. M.; Goldberg, K.; Kanazawa, A.; and Tanckic, M. 2023. Lerf: Language embedded radiance fields. In *Proceedings of the IEEE/CVF International Conference on Computer Vision*, 19729–19739.

Kirillov, A.; Mintun, E.; Ravi, N.; Mao, H.; Rolland, C.; Gustafson, L.; Xiao, T.; Whitehead, S.; Berg, A. C.; Lo, W.-Y.; et al. 2023. Segment anything. In *Proceedings of the IEEE/CVF international conference on computer vision*, 4015–4026.

Leroy, V.; Cabon, Y.; and Revaud, J. 2024. Grounding image matching in 3d with mast3r. In *European Conference on Computer Vision*, 71–91. Springer.

Li, H.; Gu, X.; Yuan, W.; Yang, L.; Dong, Z.; and Tan, P. 2023a. Dense rgb slam with neural implicit maps. *arXiv preprint arXiv:2301.08930*.

Li, M.; Liu, S.; Zhou, H.; Zhu, G.; Cheng, N.; Deng, T.; and Wang, H. 2024. Sgs-slam: Semantic gaussian splatting for neural dense slam. In *European Conference on Computer Vision*, 163–179. Springer.

Li, X.; Lin, S.; Xu, M.; Dai, D.; and Wang, J. 2021. PO-SLAM: a novel monocular visual SLAM with points and

objects. In *2021 4th International conference on artificial intelligence and big data (ICAIBD)*, 454–458. IEEE.

Li, X.; Liu, D.; and Wu, J. 2024. CTO-SLAM: contour tracking for object-level robust 4D SLAM. In *Proceedings of the AAAI Conference on Artificial Intelligence*, volume 38, 10323–10331.

Li, Z.; Müller, T.; Evans, A.; Taylor, R. H.; Unberath, M.; Liu, M.-Y.; and Lin, C.-H. 2023b. Neuralangelo: High-fidelity neural surface reconstruction. In *Proceedings of the IEEE/CVF Conference on Computer Vision and Pattern Recognition*, 8456–8465.

Lindenberger, P.; Sarlin, P.-E.; Larsson, V.; and Pollefeys, M. 2021. Pixel-perfect structure-from-motion with feature-metric refinement. In *Proceedings of the IEEE/CVF international conference on computer vision*, 5987–5997.

Liu, S.; Yu, Y.; Pautrat, R.; Pollefeys, M.; and Larsson, V. 2023. 3d line mapping revisited. In *Proceedings of the IEEE/CVF Conference on Computer Vision and Pattern Recognition*, 21445–21455.

Liu, Y.; Dong, S.; Wang, S.; Yin, Y.; Yang, Y.; Fan, Q.; and Chen, B. 2025. Slam3r: Real-time dense scene reconstruction from monocular rgb videos. In *Proceedings of the Computer Vision and Pattern Recognition Conference*, 16651–16662.

Martins, T. B.; Oswald, M. R.; and Civera, J. 2024. OVO-SLAM: Open-Vocabulary Online Simultaneous Localization and Mapping. *arXiv preprint arXiv:2411.15043*.

Mildenhall, B.; Srinivasan, P. P.; Tancik, M.; Barron, J. T.; Ramamoorthi, R.; and Ng, R. 2021. Nerf: Representing scenes as neural radiance fields for view synthesis. *Communications of the ACM*, 65(1): 99–106.

Nguyen, P.; Ngo, T. D.; Kalogerakis, E.; Gan, C.; Tran, A.; Pham, C.; and Nguyen, K. 2024. Open3dis: Open-vocabulary 3d instance segmentation with 2d mask guidance. In *Proceedings of the IEEE/CVF Conference on Computer Vision and Pattern Recognition*, 4018–4028.

Peng, S.; Genova, K.; Jiang, C.; Tagliasacchi, A.; Pollefeys, M.; Funkhouser, T.; et al. 2023. Openscene: 3d scene understanding with open vocabularies. In *Proceedings of the IEEE/CVF conference on computer vision and pattern recognition*, 815–824.

Qin, M.; Li, W.; Zhou, J.; Wang, H.; and Pfister, H. 2024. Langsplat: 3d language gaussian splatting. In *Proceedings of the IEEE/CVF Conference on Computer Vision and Pattern Recognition*, 20051–20060.

Radford, A.; Kim, J. W.; Hallacy, C.; Ramesh, A.; Goh, G.; Agarwal, S.; Sastry, G.; Askell, A.; Mishkin, P.; Clark, J.; et al. 2021. Learning transferable visual models from natural language supervision. In *International conference on machine learning*, 8748–8763. PMLR.

Ranftl, R.; Bochkovskiy, A.; and Koltun, V. 2021. Vision transformers for dense prediction. In *Proceedings of the IEEE/CVF international conference on computer vision*, 12179–12188.

Reizenstein, J.; Shapovalov, R.; Henzler, P.; Sbordone, L.; Labatut, P.; and Novotny, D. 2021. Common objects in 3d: Large-scale learning and evaluation of real-life 3d category reconstruction. In *Proceedings of the IEEE/CVF international conference on computer vision*, 10901–10911.

Schonberger, J. L.; and Frahm, J.-M. 2016. Structure-from-motion revisited. In *Proceedings of the IEEE conference on computer vision and pattern recognition*, 4104–4113.

Shotton, J.; Glocker, B.; Zach, C.; Izadi, S.; Criminisi, A.; and Fitzgibbon, A. 2013. Scene coordinate regression forests for camera relocalization in RGB-D images. In *Proceedings of the IEEE conference on computer vision and pattern recognition*, 2930–2937.

Snavely, N.; Seitz, S. M.; and Szeliski, R. 2006. Photo tourism: exploring photo collections in 3D. In *ACM siggraph 2006 papers*, 835–846.

Straub, J.; Whelan, T.; Ma, L.; Chen, Y.; Wijmans, E.; Green, S.; Engel, J. J.; Mur-Artal, R.; Ren, C.; Verma, S.; et al. 2019. The replica dataset: A digital replica of indoor spaces. *arXiv preprint arXiv:1906.05797*.

Takmaz, A.; Fedele, E.; Sumner, R. W.; Pollefeys, M.; Tombari, F.; and Engelmann, F. 2023. Openmask3d: Open-vocabulary 3d instance segmentation. *arXiv preprint arXiv:2306.13631*.

Teed, Z.; and Deng, J. 2021. Droid-slam: Deep visual slam for monocular, stereo, and rgb-d cameras. *Advances in neural information processing systems*, 34: 16558–16569.

Tie, M.; Wei, J.; Wu, K.; Wang, Z.; Yuan, S.; Zhang, K.; Jia, J.; Zhao, J.; Gan, Z.; and Ding, W. 2024. O 2 V-Mapping: Online Open-Vocabulary Mapping with Neural Implicit Representation. In *European Conference on Computer Vision*, 318–333. Springer.

Tosi, F.; Zhang, Y.; Gong, Z.; Sandström, E.; Mattoccia, S.; Oswald, M. R.; and Poggi, M. 2024. How nerfs and 3d gaussian splatting are reshaping slam: a survey. *arXiv preprint arXiv:2402.13255*, 4: 1.

Wang, F.; Zhu, Q.; Chang, D.; Gao, Q.; Han, J.; Zhang, T.; Hartley, R.; and Pollefeys, M. 2024a. Learning-based multi-view stereo: A survey. *arXiv preprint arXiv:2408.15235*.

Wang, H.; and Agapito, L. 2024. 3d reconstruction with spatial memory. *arXiv preprint arXiv:2408.16061*.

Wang, R.; Xu, S.; Dai, C.; Xiang, J.; Deng, Y.; Tong, X.; and Yang, J. 2025. Moge: Unlocking accurate monocular geometry estimation for open-domain images with optimal training supervision. In *Proceedings of the Computer Vision and Pattern Recognition Conference*, 5261–5271.

Wang, S.; Leroy, V.; Cabon, Y.; Chidlovskii, B.; and Revaud, J. 2024b. Dust3r: Geometric 3d vision made easy. In *Proceedings of the IEEE/CVF Conference on Computer Vision and Pattern Recognition*, 20697–20709.

Werby, A.; Huang, C.; Büchner, M.; Valada, A.; and Burgard, W. 2024. Hierarchical open-vocabulary 3d scene graphs for language-grounded robot navigation. In *First Workshop on Vision-Language Models for Navigation and Manipulation at ICRA 2024*.

Yeshwanth, C.; Liu, Y.-C.; Nießner, M.; and Dai, A. 2023. Scannet++: A high-fidelity dataset of 3d indoor scenes. In *Proceedings of the IEEE/CVF International Conference on Computer Vision*, 12–22.

Zhai, H.; Huang, G.; Hu, Q.; Li, G.; Bao, H.; and Zhang, G. 2024. Nis-slam: Neural implicit semantic rgb-d slam for 3d consistent scene understanding. *IEEE Transactions on Visualization and Computer Graphics*.

Zhang, J.; Herrmann, C.; Hur, J.; Jampani, V.; Darrell, T.; Cole, F.; Sun, D.; and Yang, M.-H. 2024. Monst3r: A simple approach for estimating geometry in the presence of motion. *arXiv preprint arXiv:2410.03825*.

Zhang, Y.; Tosi, F.; Mattoccia, S.; and Poggi, M. 2023. Go-slam: Global optimization for consistent 3d instant reconstruction. In *Proceedings of the IEEE/CVF International Conference on Computer Vision*, 3727–3737.

Zhu, P.; Zhuang, Y.; Chen, B.; Li, L.; Wu, C.; and Liu, Z. 2024a. Mgs-slam: Monocular sparse tracking and gaussian mapping with depth smooth regularization. *IEEE Robotics and Automation Letters*.

Zhu, S.; Qin, R.; Wang, G.; Liu, J.; and Wang, H. 2024b. Semgauss-slam: Dense semantic gaussian splatting slam. *arXiv preprint arXiv:2403.07494*.

Zhu, S.; Wang, G.; Blum, H.; Liu, J.; Song, L.; Pollefeys, M.; and Wang, H. 2024c. Sni-slam: Semantic neural implicit slam. In *Proceedings of the IEEE/CVF Conference on Computer Vision and Pattern Recognition*, 21167–21177.

Zhu, Z.; Peng, S.; Larsson, V.; Cui, Z.; Oswald, M. R.; Geiger, A.; and Pollefeys, M. 2024d. Nicer-slam: Neural implicit scene encoding for rgb slam. In *2024 International Conference on 3D Vision (3DV)*, 42–52. IEEE.

Zuo, X.; Samangouei, P.; Zhou, Y.; Di, Y.; and Li, M. 2025. Fmgs: Foundation model embedded 3d gaussian splatting for holistic 3d scene understanding. *International Journal of Computer Vision*, 133(2): 611–627.